Using cavitation as a probe of low-pressure filaments in turbulence

Frédéric Moisy[1], Arthur La Porta[2], Greg Voth[2], and Eberhard Bodenschatz[2]

[1] Laboratoire de Physique Statistique, ENS, 24 rue Lhomond, F-75231 Paris Cedex 05

[2] Laboratory of Atomic and Solid State Physics, Cornell University, Ithaca, New York 14853-2501

Abstract. We report new observations of low-pressure filaments in a turbulent flow between counter-rotating disks [1]. Cavitation from microscopic gas bubbles seeding the water is used to probe the structure of the pressure field. The spatial structure of the low-pressure events, mainly vertical filaments standing along the disks axis, are visualized using a high speed video system. The negative tail of the probability density functions of pressure is determined from light scattering measurements performed with a fast photo detector, and is found to be exponential. These observations highlight the importance of the large scales on the pressure fluctuations.

1 Introduction

The importance of vortex structures with concentrated vorticity in turbulent flows has been recognized for a long time. Direct numerical simulations of homogeneous and isotropic turbulence clearly show that the most intense of these vortex filaments, the so-called worms [2,3], are responsible for the non-gaussian statistics of velocity derivatives [4]. Moreover, worms are also found to be responsible for the skewed pressure distributions [5], although this can not really be viewed as a signature of structures in the flow.

The basic idea of the experiment described here arises from the link between high vorticity regions and local pressure minima *via* the Poisson equation

$$\frac{2}{\rho}\nabla^2 p = \omega^2 - \sigma^2$$

for an incompressible fluid (of density ρ), where ω^2 and σ^2 are the squared vorticity and rate of strain tensors. This link, highlighted by Brachet (1990) [6], has motivated several experiments [7,8], where migration of gas bubbles against the pressure gradient allows visualization of low-pressure regions in turbulent water flows. However, quantitative pressure measurements usually suffer from the invasive character of conventional sensors [9,10]. For this reason, such measurements are usually performed by probes mounted on the walls [11,12], and little is known about the pressure field in the bulk of turbulent flows.

In order to provide information about pressure fluctuations in the case of liquids, it is tempting to use cavitation. Cavitation in low pressure vortices has been extensively studied in the context of fluid machinery [13–16]. Arndt [13]

shows how the pressure inside the vortex core can be estimated from cavitation inception. Ran and Katz [17,18] show that it is possible to obtain a non intrusive pressure measurement from (non cavitating) bubble size measurements.

In the experiment we present here, we make use of cavitation to investigate both the structural organization and the statistics of pressure fluctuations in the turbulent flow between counter-rotating disks. Cavitation is triggered where small air bubbles seeding the flow enter in regions where the local pressure becomes below a fixed pressure threshold. This pressure threshold is given by the vapor pressure and a surface tension correction due to the air bubble size seeding the flow. The purpose of this paper is to focus on the large scale properties on the flow in this geometry, while the results reported in La Porta *et al* [1] detail the statistical aspects.

2 Experimental set-up

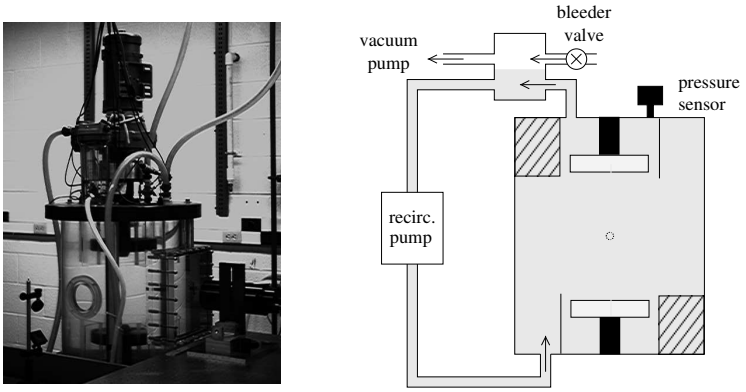

Fig. 1. Left: Picture of the experimental apparatus. Right: Pressure control system. The dashed circle in the center represents the 3 cm^3 imaged region used in section 5.

The turbulent flow we study takes place in a 110 L water tank, driven by two counter-rotating disks (see figure 1). A large plane window is mounted on the side to allow undistorted visualization, and a smaller circular one at 90^o for illumination. The disks are open-ended cylinders, 20 cm in diameter and 4.3 cm heigh, with twelve radial vanes to provide efficient stirring. They are spaced 33 cm apart, driven by two electronically controlled DC motors, spanning a frequency rate ranging from 0 to 9 Hz within $\pm$ 1%. More experimental details can be found in Voth *et al* [19] and La Porta *et al* [1].

In order to use cavitation to probe the pressure field, it is crucial to control precisely the mean hydrostatic pressure; this is achieved using the arrangement shown in figure 1. It consists of an auxiliary chamber, mounted above the main fluid volume, both two being included in a recirculating loop. Pumping on the

water/air interface in the auxiliary chamber, and adjusting the air flow rate through a servo controlled bleeder valve, allows us to finely regulate the hydrostatic pressure in the main tank. Pressure fluctuations have to be large enough to generate significant cavitation, imposing a minimum frequency rate of 7 Hz. Table 1 sums up the flow characteristics for frequency rates of 7, 8 and 9 Hz. The mean hydrostatic pressure, noted p_0, is taken at the center of the flow, and includes the shift from the top to the center, $\rho gh = 30$ mbar.

f (Hz)	Re $=\Omega R^2/\nu$	τ_η (ms)	η (μm)	λ (mm)	$\frac{1}{2}\rho U_d^2$ (mbar)	R_λ
7	$4.40 \cdot 10^5$	0.67	26	2.12	96	1658
8	$5.03 \cdot 10^5$	0.54	23	1.99	126	1772
9	$5.65 \cdot 10^5$	0.45	21	1.89	160	1880

Table 1. Range of turbulence parameters. The disk velocity U_d is given by $2\pi Rf$, where R =10 cm is the disk radius. Values of the Taylor scale (λ), Kolmogorov scales (η, τ_η) and microscale Reynolds number (R_λ) are determined from measurements in the center of the flow [19].

The mean flow between counter rotating disks can be seen as the superposition of two components, a pumping mode and a shearing mode. Fluid near the top and the bottom rotates with the disks, producing a shear layer in the mid plane. Additionally, the axial pumping and the radial ejection, due to the disk rotation, creates two toroidal recirculation rolls. The mean velocity of this pumping mode has been estimated by a position sensitive detector, and is found to be around 20% of the maximum azimuthal velocity.

The flow is illuminated using light sources at 90^o, and low-pressure events are detected as light scattered from cavitating bubbles. Two imaging systems have been used:

- Qualitative characterization of the low-pressure events is achieved by recording scattered light with a 400 Hz video camera . The exposure time is given by the sampling rate when continuous illumination is used (tungsten lamp), but it can be decreased down to 20 μs using a stroboscopic illumination, synchronized with the video system. These observations are described in section 4.
- In order to extract more quantitative information about the probability density function of the pressure fluctuations, a 30 kHz PIN photodiode collects light scattered from a 3 cm^3 central circular area. Assuming cavitation is triggered when local pressure reaches a given threshold, we show, in section 5, how pressure statistics can be deduced from the fraction of the time that cavitation occurs.

Both pure and salted water have been used to perform the visualization. Salted water (0.27 mol/L NaCl) makes the air microbubbles more stable, and

allows to decrease the hydrostatic pressure further in order to visualize weaker filaments. The quantitative measurements presented in section 5 have been performed only in pure water, but consistent results have been obtained in salted water.

3 Using cavitation bubbles as pressure sensors

In the following we only discuss the case of cavitation in pure water, from which quantitative information on the pressure fields has been obtained. The salted water case seems to be much more complex — the bubbles seem to be more stable, and less likely to cavitate or coalesce.

Pure cavitation is expected to occur when the local pressure in a liquid goes below the vapor pressure: a vapor bubble will grow by conversion of liquid to vapor at the bubble interface [20]. However, the surface tension energy needed to nucleate an arbitrary small vapor bubble from pure liquid water considerably decreases this pressure threshold. In most of the cases, cavitation occurs from impurities, the roughness of the wall, or pre-existing microbubbles in the water, allowing to reach the surface tension barrier.

In our set-up, water is finely purified and cavitation in the center of the flow arises from air microbubbles seeding the water. In the absence of disks rotation, examination with a long working distance microscope shows that the radius of these stable air bubbles is 35 ± 10 µm. Note that this value is of the order of the Kolmogorov scale, ranging from 21 to 26 µm (see table 1). Assuming that the air filling the seeding bubbles behaves as an isothermal ideal gas [17], we can deduce the cavitation pressure threshold:

$$p_c \simeq 20 \text{ mbar}. \tag{1}$$

We note that this value is close to the the water vapor pressure ($p_v = 29$ mbar at 25^oC). Migration of gas bubbles into low-pressure regions precedes cavitation of vapor bubbles, a mechanism already noted by Ran and Katz [18].

In turbulent flows, the pressure distribution is believed to be negatively skewed [5]; the most negative pressure drops locally reach the well defined pressure threshold (1) and trig cavitation. In our experiment, for small cavitation rate (*i.e.* for high hydrostatic pressure), cavitation can be considered as a passive trigger of low pressure regions. Vapor bubbles are indeed unstable and quickly collapse after their nucleation from the seeding bubbles. In this case, cavitation consists essentially of brief flashes of light scattering. A reasonable timescale of the growth and collapse process can be estimated from the resonant frequency of the air bubbles, around 100 µs for the 35 µm radius bubble (see the Ref. [17] for a detailed study of the time response of a gas bubble). This time scale is then found to be lower than the Kolmogorov timescale (around 500 µs, see table 1), allowing us to consider that cavitation is triggered instantaneously by pressure fluctuations. Of course, the same does not go for higher cavitation rates (lower hydrostatic pressure), where big vapor cavities are found to fill the vortex cores [13]. Indeed, vapor bubbles' response time can be much higher, and it is only for low cavitation rates that cavitation can be seen as a passive trigger.

4 Visualization of coherent structures

The large scale structure of the flow is observed using the high speed video system, by setting the hydrostatic pressure slightly above the pressure threshold ($p_0 \simeq 70$ to 120 mbar). At the lowest hydrostatic pressure, cavitation bubbles are created at a high rate throughout the fluid volume, leading to a high density of stable gas bubbles seeding the flow. In this case, visualization is due to cavitation itself, as well as migration of gas bubbles towards local minima of the pressure. For higher hydrostatic pressure, the small seeding gas bubbles are trapped into the vortex core, increasing the cavitation likelyhood. However, in this case, gas bubbles are not detected by our imaging system and visualization is only due to cavitation of vapor bubbles from the preexisting nuclei.

Fig. 2. Few cavitating bubbles aligned along a vertical filament, in stroboscopic lighting (exposure time 20 µs), vertical field of view is 6.8 cm. From one picture to the other one, vapor bubbles are different but clearly cavitate from the same region.

Cavitation highlights regions of low pressure in three regions :

- In the center, mostly long vertical filaments are shown. Their length can reach 10 cm, and their mean life time is about 30 ms, up to 100 ms, of the order of the turnover time $1/f \simeq 110$ to 140 ms. Their diameter can be estimated around 2 mm. This value is found to be close to the Taylor scale (see table 1), however the scaling with Reynolds number can not be tested. At high hydrostatic pressures, when only the deepest depression trigger cavitation, these events appear less often and only consist in a few bubbles, aligned along a vertical "necklace" (see figure 2).
- Near the central shear layer, more disorganized flame-like cavitation events appear from periphery to the center. Sometimes they roll up, leading to a well defined horizontal filaments, advected to the center. The mean waiting time between such events can also been estimated to $1/f \sim 100$ ms.
- At last, we can mention that cavitation also occurs near the blades of the disks, seeding the flow with disorganized sprays of air microbubbles. Careful observations reveal the existence of strong localized vortices between each blades, moving together with the disks (see figure 3). However, because of the high velocity at the periphery of the disks, we believe that there is no link between these blades vortices and the long vertical filaments in the center of the flow.

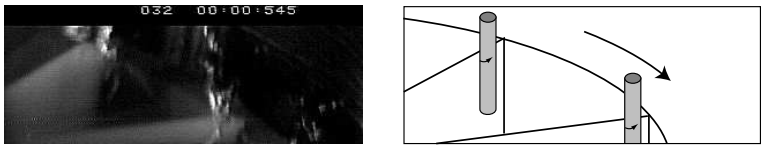

Fig. 3. Picture and sketch of stable vortices localized between each disk blade.

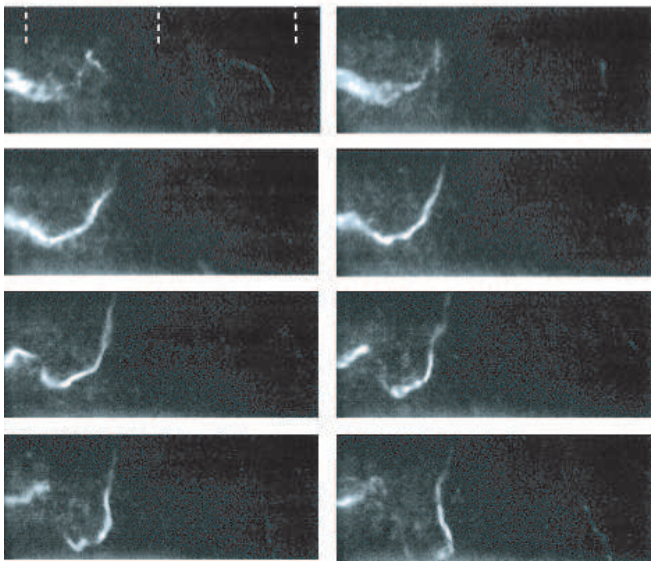

Fig. 4. Standing up of a filament, created on the horizontal shear layer (on the left), and advected upward. Dashed lines on the first picture indicates the center and the borders of the disks. Continuous lighting in salted water, the horizontal field of view is 23 cm.

The first and second observations lead us to suggest a mechanism of formation and amplification of the filaments: The shear layer rolls up from a (radial) Kelvin-Helmholtz instability, leading to horizontal filaments. This filaments stand up to the center of the flow, advected by the mean recirculation flow and stretched by the mean radial and axial strain, leading to the strong vertical filaments observed in the center (see figure 4, sketched on figure 5). Both the mean waiting time and the mean life time ($\simeq 1/f$) suggest that large scale features are responsible of the formation and amplification of these objects.

The maximum hydrostatic pressure $p_0(max)$ for which first cavitation events appear gives an estimation of the typical depression associated to the strongest

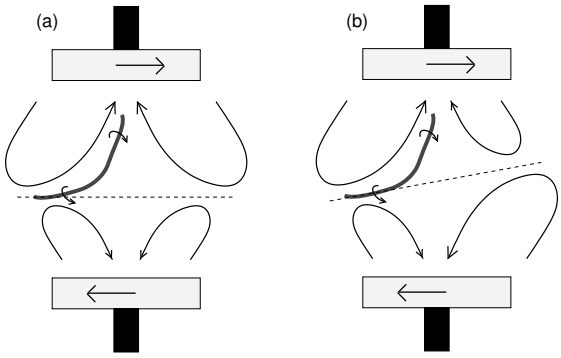

Fig. 5. Scenario of standing up of a filament. The unstable shear layer shifts (a) or tilts (b) (dashed line), on timescale of one or a few turnover times.

filaments. The so-called cavitation inception index,

$$\sigma_i = \frac{{p_0}^{(max)} - p_c}{\frac{1}{2}\rho {U_d}^2},$$

is a rough measure of the strongest depression giving rise to cavitation, compared to the typical large-scale pressure $\frac{1}{2}\rho U_d^2$ (see the values in table 1). This index is found to lie roughly between 1.2 and 1.5 (with a slight trend to increase with the Reynolds number), meaning that the strongest depressions are controlled by the largest scales. From this observation it is clear that the azimuthal velocity of the strongest filaments is of the order of the disk velocity, *i.e.* the highest velocity injected in the flow. This is found to be qualitatively consistent with other investigations in different flow configurations [13]. It is also in good agreement with the wall measurements of Fauve (1993) [21] and Cadot (1995) [12].

Lower hydrostatic pressures allow to investigate weaker filaments, whose depression are less deep. Observations in this regime reveal a population of smaller filaments, apparently more isotropically distributed. We can suppose that these weaker filaments are less affected by the large scale features of the flow.

Destabilization of filaments can be investigated using salted water in this low pressure regime. Making bubbles more stable and less likely to coalesce, it allows to keep track of the structures even if their depression increase. Sometimes destabilization appears to be due of helical undulations, self-advected along the vortex axis, whose typical wavelength seems to decrease until the vortex looses coherence (see figure 6).

Vertical filaments at the center of the flow are sometimes observed to cluster in braid-like structures. The figure 7 shows two filaments, mutually advected and orbiting around each other. There is no evidence of link between these braid-like structures and destabilization nor smaller filaments.

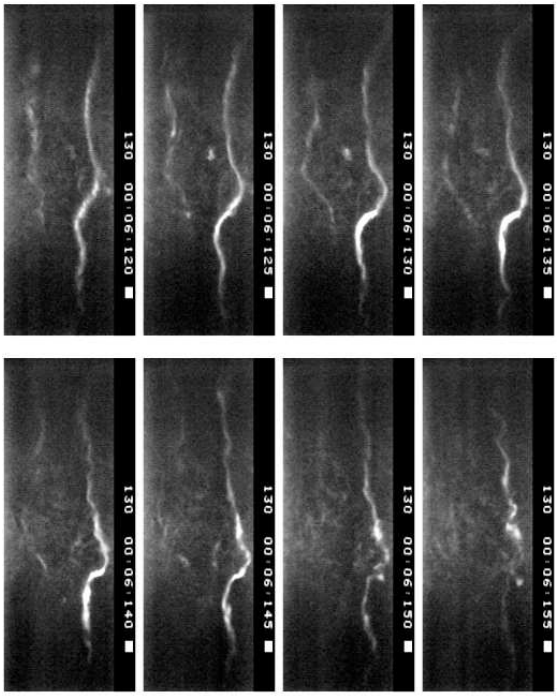

Fig. 6. Large vertical filament undergoing undulations, leading to its destabilization. The vertical field of view is 16 cm, and the time interval between frame is 5 ms.

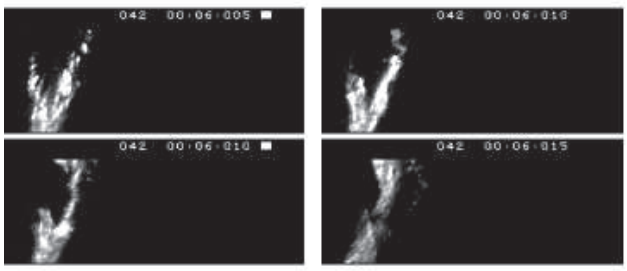

Fig. 7. Sequence showing two braids rotating around each other. Continuous lighting. The horizontal field of view is 8 cm, and the time interval between frame is 2.5 ms.

5 Statistics of cavitating events

In this section we briefly describe how statistics of the pressure fluctuations can be deduced from measurements of the light scattering from the cavitating bubbles. The basic idea is that the air microbubbles are stable at the mean pressure and not detectable by the photo detector (or at least account for the

noise level), but they explode when enter a region where the pressure is below the cavitation threshold p_c and light scattering from this cavitating bubbles is detected. The easiest way to relate the level of cavitation activity at a given hydrostatic pressure to the fluctuation pressure distribution is to assume the black-and-white scheme:

$$p(\mathbf{x},t) \leq p_c \Rightarrow \text{ cavitation}$$
$$p(\mathbf{x},t) \geq p_c \Rightarrow \text{ no cavitation.}$$

Synchronized measurements with the photo detector and the video system used in the previous section gave evidence that the measured light signal corresponds to the presence of cavitating bubbles.

We define the *cavitation on-fraction* as the fraction of the time that cavitation is occurring in the 3 cm^3 central region (see figure 1). Indeed, in the limit of small volume, this cavitation on-fraction at a given hydrostatic pressure p_0 is given by

$$\wp(p \leq p_c; p_0) \propto \int_{-\infty}^{p_c} f(p; p_0)\, dp, \tag{2}$$

where $f(p; p_0)$ is the pressure probability density function (pdf), satisfying $\langle p \rangle = p_0$. Thus, varying the hydrostatic pressure p_0, we adjust the distance to the cavitation threshold $p_0 - p_c$, and we are able to measure point by point this cumulative distribution function $\wp(p \leq p_c; p_0)$.

From the light collected by the photo detector we have computed the cavitation on-fraction (2), following a procedure described in La Porta *et al* [1]. These curves are well fit by exponential, meaning that the pressure pdf, given by (minus) the on-fraction derivative, can be written

$$f(p; p_0) \sim e^{-(p-p_0)/\alpha}, \tag{3}$$

where the pressure constant α in $f(p; p_0)$ is the same as the one in $\wp(p \leq p_c; p_0)$. We obtain from best fit α =26.6, 35.4 and 48.1 mbar, for frequency rates f =7, 8 and 9 Hz, an increase reflecting the widening of the pressure pdf with increasing Reynolds number.

Other statistical measures, bridging from cavitation activity to pressure pdfs, are also discussed in the Ref. [1]. One is the cavitation waiting time between bursts of high activity level, and can be roughly seen as the complementary of the cavitation on-fraction, since the fraction of time that cavitation is *not* occurring is given by the average of the waiting time distribution. These methods lead to the same observation of an exponential distribution of pressure fluctuations.

In order to check the similarity of these pressure pdfs for different Reynolds numbers, we should rescale them by the pressure variance. However, this quantity is not measurable from cavitation, since the procedure described above is only supposed to work for extreme negative fluctuations. Assuming similarity, the pressure variance is expected to scale as $\rho U^2 \sim \text{Re}^2$. The figure 8 collects the values of the pressure constant α for the three different Reynolds numbers. Although the range of Reynolds number available is too small to provide a strong

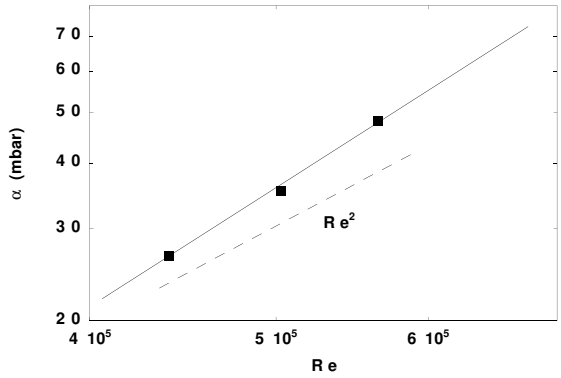

Fig. 8. Scaling of the pressure constant, as defined in (3), of the cavitation on-fraction with the Reynolds number. The dashed lines indicate the expected Re^2 scaling, and the straight line is a best fit by a power law, $\mathrm{Re}^{2.3}$.

test of the scaling, a linear fit to the log-log plot indicates that the pressure constant scales as $\mathrm{Re}^{2.3}$, slightly faster than the expected Re^2. However, the similarity scaling can not been ruled out, because self-seeding effects of cavitation may increase the cavitation activity level at higher Reynolds numbers, introducing a systematic bias for this measure.

6 Discussion and conclusion

We have shown that cavitation can be a useful tool to probe locally the turbulent fluctuating pressure in the bulk, allowing to visualize the structures resulting from a spatial cut in the pressure field at a well defined threshold close to the vapor pressure. Moreover, when the cavitation rate is low enough, this method allows to deduce statistics of the pressure fluctuations, usually not available from non invasive bulk measurement.

Our observations lead us to the conclusion that these structures can be seen as *large scale* objects:

- Their length, of the order of the disk diameter, and their orientation, along the vertical axis, suggest that these objects are essentially controlled by the large scales of the flow, even at very high Reynolds number.
- Their maximal azimuthal velocity is of the order of the disks velocity $U_d = 2\pi Rf$ (where R is the disk radius), and the corresponding depression $\sim \rho U_d^2$. Here again the filament characteristics are controlled by the large scale velocity U_d and *not* by the Kolmogorov velocity scale $\sim U_d(r/R)^{1/3}$.
- Both their life time and mean waiting time are of the order of the turnover time $1/f$. This timescale is related to their mechanism of formation (shear layer instability) and amplification (axial stretching due to the centrifugal pumping), which are properties of this specific stirring geometry.

These conclusions are in good agreement with other studies [8,22]: these low-pressure filaments appear to be the trace of primary instabilities of this flow, rather than turbulence itself. However, we have noted that visualizations of migrating bubbles at very low hydrostatic pressure revealed the existence of weaker filaments, whose orientation seems to be more randomly distributed. This suggests that weaker filaments are less sensitive to the large scales of the flow.

Additionally, statistics of scattering light from cavitation allow us to reconstruct the negative tail of the pressure pdf, in the central region of the flow where strongly anisotropic filaments are observed. These tails are found to decrease exponentially, with pressure constant scaling roughly as Re^2, in agreement with similarity hypothesis (discrepancy from this scaling may be due to the self-seeding effect of cavitation). Together with the previous observations, this means that the far tails of the exponential pressure distributions are controlled by the strongest, anisotropic, filaments, whereas the weaker ones contribute to an intermediate range of these distributions.

These observations raise the issue of the *universality* of pressure fluctuations in turbulence. Are our exponential distributions related to the ones observed in numerical simulations [5,23]? Pumir (1994) [5] notes that, in isotropic and homogeneous numerical turbulence, the lowest depressions are due to the worms [2,3], small scale vortices, whose radius is of the order of the Kolmogorov scale. Shall we conclude that, in an inhomogeneous and anisotropic case, depressions due to the large scale vortices hide the more *universal* properties of smaller scale pressure fluctuations?

The authors acknowledge P. Tabeling, H. Willaime and J.S. Andersen for fruitful discussions.

References

1. A. La Porta, G.A. Voth, F. Moisy and E. Bodenschatz: Using cavitation to measure statistics of low-pressure events in large-Reynolds-number turbulence, submitted to *Phys. Fluid* (1999). Preprint available on `http://milou.msc.cornell.edu/publications.html`.
2. F. Belin, J. Maurer, P. Tabeling, and H. Willaime: Observation of intense filaments in fully developed turbulence, *J. Phys II* **6**, 573–584 (1996).
3. J. Jimenez: Small scale intermittency in turbulence *Eur. J. Mech. B/Fluids* **17** (4), 405–419 (1998).
4. E.D. Siggia: Numerical study of the smale-scale intermittency in three-dimensional turbulence, *J. Fluid. Mech.* **107** (3), 375–406 (1981).
5. A. Pumir: A numerical study of pressure fluctuations in three-dimensional, incompressible, homogeneous, isotropic turbulence *Phys. Fluids* **6** (6), 2071–2083 (1994).
6. M.E. Brachet: The geometry of small-scale structures of the Taylor-Green vortex, *C.R.Acad.Sci.Paris* **311**, 775–780 (1990).
7. S. Douady, Y. Couder, and M.E. Brachet: Direct observation of the intermittency of intense vorticity filaments, *Phys. Rev. Lett* **67**, 983–986 (1991).
8. E. Villermaux and Y. Gagne: Intense vortical structures in grid-generated turbulence *Phys. Fluids* **7** (8), 2008–2013 (1995).

9. W.K. George, P.D. Beuther and R.E.A. Arndt: Pressure spectra in turbulent free shear flows *J. Fluid. Mech.* **148**, 155–191 (1984).
10. F. Moisy and P. Petitjeans: Pressure measurements in a stretched vortex, in this Volume.
11. P. Abry, S. Fauve, P. Flandrin, and C. Laroche : Analysis of pressure fluctuations in swirling turbulent flows *J. Phys. II France* **4** 725–733 (1994).
12. O. Cadot, S. Douady, and Y. Couder: Characterisation of the low pressure filaments in a 3D turbulent shear flow, *Phys. Fluids* **7**, 630–646 (1995).
13. R.E.A. Arndt: Cavitation in fluid machinery and hydraulic structures *Ann. Rev. Fluid. Mech.* **13**, 273–328 (1981).
14. T.J. O'Hern: An experimental investigation of turbulent shear flow cavitation, *J. Fluid. Mech.* **215**, 365–391 (1990).
15. B. Belahadji, J.P. Franc and J.M. Michel:Cavitation in the rotational structures of a turbulent wake *J. Fluid. Mech.* **287**, 383–403 (1995).
16. O. Boulon, M. Callenaere, J.P. Franc and J.M. Michel: An experimental insight into the effect of confinement on tip vortex cavitation of an elliptical hydrofoil, *J. Fluid. Mech.* **390**, 1–23 (1999).
17. B. Ran and J. Katz: The response of microscopic bubbles to dussen changes in the ambiant pressure *J. Fluid. Mech.* **224**, 91–115 (1991).
18. B. Ran and J. Katz: Pressure fluctuations and their effect on cavitation inception within water jets *J. Fluid. Mech.* **398**, 1–43 (1999).
19. G.A. Voth, K. Satyamarayan and E. Bodenschatz: Lagrangian Acceleration Measurements at Large Reynolds Numbers, *Phys. Fluids* **10** (9), 2268–2280 (1998).
20. M.S. Plesset and A. Prosperetti: Bubble dynamics and cavitation *Ann. Rev. Fluid. Mech.* **9**, 145–185 (1977).
21. S. Fauve, C. Laroche and B. Castaing: Pressure fluctuations in swirling turbulent flows *J. Phys. II France* **3**, 271–278 (1993).
22. S. Fauve, S. Aumaitre, P. Abry, J.-F. Pinton, and R. Labbe: Large scale fluctuations in swirling flows, Advances in Turbulence VII, Kluwer Ac. Publishers, Uriel Frisch Ed. (1998).
23. V. Prakash and P.K. Yeung: Similarity scaling of acceleration and pressure statistics in numerical simulations of isotropic turbulence, *Phys. Fluids* **11**, 1208–1220 (1999).